J Nanopart Res (2012) 14:988
DOI 10.1007/s11051-012-0988-0

RESEARCH PAPER

Synthesis and characterization of polyvinylimidazole-grafted superparamagnetic iron oxide nanoparticles (Si-PVIm-grafted SPION)

H. Erdemi · H. Sözeri · M. Şenel · A. Baykal

Received: 26 April 2012 / Accepted: 11 June 2012 / Published online: 3 July 2012

Abstract Polyvinylimidazole (PVIm)-grafted superparamagnetic iron oxide nanoparticles (SPION) (Si-PVIm-grafted Fe_3O_4 NPs) were prepared by grafting of telomere of PVIm on the SPION. The product identified as magnetite, which has an average crystallite size of 9 ± 2 nm as estimated from X-ray line profile fitting. Particle size was estimated as 10.0 ± 0.5 nm from TEM micrographs. Mean particle size is found as 8.4 ± 1.0 nm which agrees well with the values calculated from XRD patterns (9 ± 2 nm). Vibrating Sample Magnetometer (VSM) analysis explained the superparamagnetic nature of the nanocomposite. Thermogravimetric analysis showed that the Si-Imi is 25 % of the Si-PVIm-grafted SPION, which means an inorganic content is about 75 %. Detailed electrical and dielectric properties of the properties of the product are also presented. The conductivity of the sample increases significantly with temperature and has the value in the range of 1.14×10^{-7}–1.78×10^{-4} S cm^{-1}. Analysis of the real and imaginary parts of the permittivities indicated temperature and frequency dependency representing interfacial polarization and temperature-assisted reorganization effects.

Keywords SPION · Magnetic nanomaterials · Conductivity · Permittivity · Magnetization · Electrical properties

H. Erdemi
Department of Polymer Engineering, Yalova University, 77100 Yalova, Turkey

H. Sözeri
National Metrology Institute, TUBITAK-UME, PO Box 54, 41470 Gebze, Kocaeli, Turkey

M. Şenel · A. Baykal (✉)
Department of Chemistry, Faculty of Arts and Sciences, Fatih University, B.Cekmece, Istanbul 34500, Turkey
e-mail: hbaykal@fatih.edu.tr

Introduction

Recently functionalized nanomaterials have gained importance due to their unusual optical, electrical, and molecular properties which find numerous technological applications including those in biomedical industries (Bajaj et al. 2010). Surface modification by graft polymerization is a versatile method for the molecular design of solid surfaces to enhance their physical and chemical properties for specific applications (Takafuji et al. 2004). Surface modification of magnetic particles by organic compounds can be achieved via four major avenues: organic vapor condensation, polymer coating, surfactant adsorption, and direct silanation of silane-coupling agents (Takafuji et al. 2004).

In addition to colloidal stability and shelf-life, surface functionalization also plays a prominent role in defining a nanostructure's behavior in the target system, including cellular internalization, targeting, epsonization, and bio-compatibility.

Well-defined polymer brushes can be incorporated on substrate surfaces via robust covalent bonds to render the surface with excellent mechanical and chemical protection, alter the electrochemical characteristics of the interface, and provide new surface functionality (Yuan et al. 2010; Deligöz et al. 2012a, b; Aydin et al. 2012; Paulsen et al. 2004). Polymer coatings can enhance compatibility with organic ingredients, reduce susceptibility to leaching, and protect particle surfaces from oxidation. Encapsulation or dispersion of magnetic nanoparticles into organic polymers to form magnetic composites endows materials with some important properties that bare uncoated particles lack (Deligöz et al. 2012b).

Silica coating on the surface of nanosize iron oxide particles, for example, could help prevent their aggregation in liquids, improve their chemical stability, and control of surface properties (Butterworth et al. 2001). Silica is a nontoxic and biocompatible material and has been widely used to improve the stability of nanoparticles in a basic environment (Nishio et al. 2007; Yang et al. 2010; Setyawan et al. 2012). Silica is surface terminated with silanols (–SiOH), allowing for silica-coated magnetite nanoparticles can be easily modified with many functional groups, such as amines, thiols, and carboxyl groups. This covalent modification of the particle surfaces with biological molecules, such as drugs, proteins, enzymes, antibodies, or nucleotides, creates magnetite nanoparticles that can be used for biomedical applications (Kim et al. 2003).

It is known that the polymer with terminal reactive groups can be grafted onto a surface of inorganic materials, and this grafting technique allows applications of the hybrid materials to many important fields (Takafuji et al. 2004; Kim et al. 2003; Vogt et al. 2010; De et al. 2011). Excellent features of the ferrite/polymer composites make them quite attractive for applications not only as inductive and capacitive materials but also as microwave absorber materials. These characteristics are related to a sharply reduced dielectric loss compared to that of bulk ferrites (Kavas et al. 2010). Takafuji et al. (2004) synthesized the poly(1-vinylimidazole)-grafted magnetic nanoparticles for the removal of metal ions. Yuan et al. (2010) prepared the poly(1-vinylimidazole)-grafted copper surface that improves the corrosion resistance of copper. Poly(1-vinyl-1,2,4-triazole) (PVTri)–Fe_3O_4 nanocomposite with conducting character was synthesized via wet chemical process by Kavas et al. (2010).

The main purpose of this study is the synthesis and characterization of polyvinylimidazole-grafted superparamagnetic iron oxide nanoparticles (Si-PVIm-grafted SPION). To the best of our knowledge, this study is the first for the fabrication, magnetic, and electrical evaluation of Si-PVIm-grafted SPION. The product was evaluated for its physicochemical, magnetic, conductivity, and dielectric permittivity properties, and evaluation results are presented in detail.

Experimental

Materials and instrumentation

Ferric chloride hexahydrate, ferrous chloride tetrahydrate, 1-vinylimidazole (VIm), 3-mercaptopropyltrimethoxysilane (MPS), and 2,2′-azobis (isobutyronitrile) (AIBN) were purchased from Fluka and Across Chemical Co. and used without further purification. All other chemicals were of analytical grade and were used without further purification.

X-ray powder diffraction (XRD) analysis was conducted on a Rigaku Smart Lab Diffractometer operated at 40 kV and 35 mA using Cu K_α radiation.

High-resolution transmission electron microscopy (HR-TEM) analysis was performed using a JEOL JEM 2100 microscope. A drop of diluted sample in alcohol was dripped on a TEM grid.

Fourier transform infrared (FT-IR) spectra were recorded in transmission mode with a Perkin Elmer BX FT-IR infrared spectrometer. The powder samples were ground with KBr and compressed into a pellet. FT-IR spectra in the range of 4000–400 cm^{-1} were recorded in order to investigate the nature of the chemical bonds formed.

The thermal stability was determined by thermogravimetric analysis (TGA, Perkin Elmer Instruments model, STA 6000). The TGA thermograms were recorded for 5 mg of powder sample at a heating rate of 10 °C/min in the temperature range of 30–800 °C under nitrogen atmosphere.

VSM measurements were performed using a vibrating sample magnetometer (LDJ Electronics Inc., Model 9600). The magnetization measurements were carried out in an external field up to 15 kOe at room temperature.

The electrical properties of the product were studied in the temperature range of 20–120 °C with a heating rate

of 10 °C/s. The sample was used in the form of circular pellets of 13 mm diameter and 3 mm thickness. The pellets (both nanocomposite and pristine) were sandwiched between gold electrodes, and the conductivities were measured using novocontrol dielectric impedance analyzer in the frequency range of 1 Hz–3 MHz, respectively. The temperature (between −100 and 250 °C) was controlled with a Novocool Cryosystem.

Preparation of Fe_3O_4 (MNP)

An aqueous suspension of Fe_3O_4 was prepared using controlled co-precipitation method as reported earlier (Uzun et al. 2010). Briefly, 25 mL of 1 M $FeCl_3 \cdot 6H_2O$, 0.5 M $FeCl_2 \cdot 4H_2O$, and 0.4 M HCl was prepared as a source of iron by dissolving the respective chemicals in Milli-Q water under vigorous stirring. The co-precipitation of MNP was carried out in a reactor with high-speed mechanical stirring (2,000 rpm) by adding the iron solution to 250 mL of 0.5 M NaOH, which was preheated to 80 °C before the co-precipitation reaction. N_2 was used during the reaction to prevent critical oxidation. Black powder was collected by sedimentation with a help of an external magnetic field and washed several times with Milli-Q water until stable ferrofluid was obtained. Finally, the superparamagnetic nanoparticles were re-dispersed in an aqueous solution by changing the pH to 11 with TMAOH (5 wt%).

Preparation of poly(1-vinylimidazole) (Si-PVIm)

Telomerization of poly(1-vinylimidazole) was accomplished by dissolving 1-vinylimidazole monomer (50 mmol) and MPS (2 mmol) in benzene (10 mL), followed by the addition of 2 wt% AIBN (Takafuji et al. 2004). The mixture was degassed using Argon gas and sealed under vacuum. After degassing, the tubes were placed in constant temperature baths controlled to 80 °C. After 2 days, white precipitates were formed upon the addition of diethyl ether to the residue solution at −20 °C. Precipitated copolymer was washed with diethyl ether and re-precipitated in this manner two more times. Precipitated product was then dried under vacuum.

Silanization of MNP

The synthesized Si-PVIm was silanized onto nanosize magnetic particles in toluene/methanol (with volume ratio of 80:20) solution at the reflux temperature for 2 days (Fig. 1). The silanized particles were washed repeatedly with organic solvents and collected by centrifugation. After washing, the particles were dried in vacuum.

Result and discussion

XRD analysis

Phase investigation of the crystalline product was performed by XRD, and the diffraction pattern is presented in Fig. 2. The XRD pattern indicates that the product consists of magnetite, Fe_3O_4, and the diffraction peaks are broadened owing to very small crystallite size. All of the observed diffraction peaks are

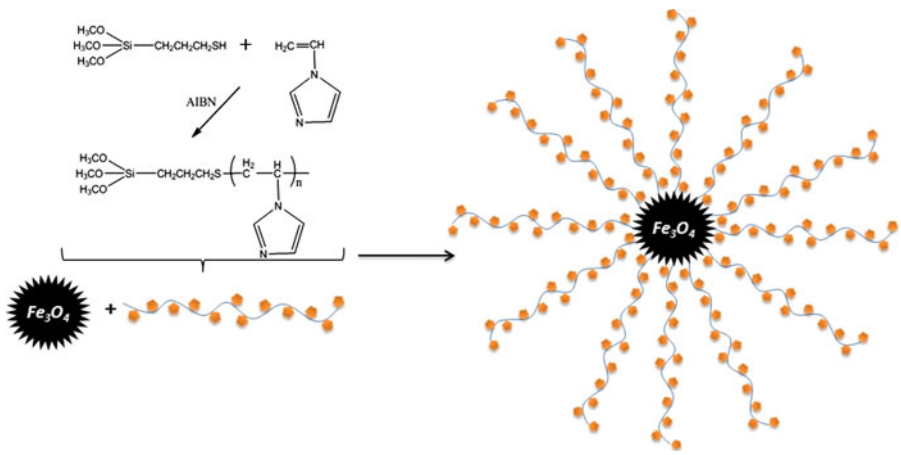

Fig. 1 Synthesis of Si-PVIm-grafted SPION

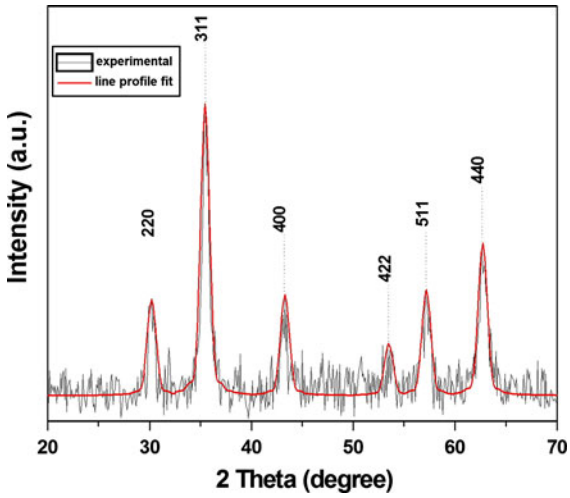

Fig. 2 XRD powder pattern and line profile fitting of Si-PVIm-grafted SPION

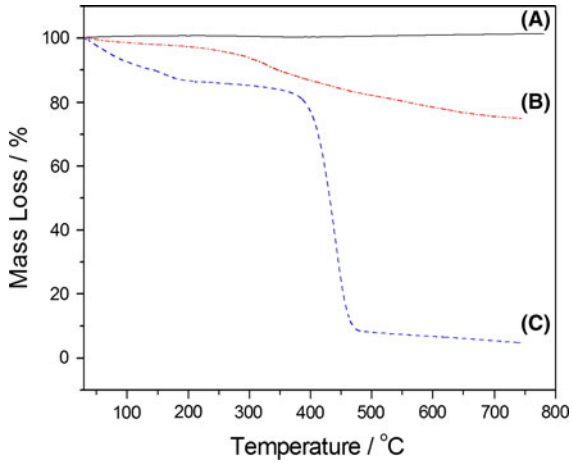

Fig. 3 TGA thermograms of **a** pure Fe_3O_4, **b** Si-PVIm-grafted SPION, and **c** Si-Imi

indexed by the cubic structure of Fe_3O_4 (JCPDS No. 19-629) revealing a high-phase purity of magnetite. The mean size of the crystallites was estimated from the diffraction pattern by line profile fitting method using Eq. 1 (Wejrzanowski et al. 2006; Pielaszek 2003). The line profile shown in Fig. 2 was fitted for observed six peaks with the following miller indices: (220), (311), (400), (422), (511), and (440). The average crystallite size, D and σ, was obtained as 9 ± 2 nm as a result of this line profile fitting.

Thermogravimetric analysis

TGA curves of pure Fe_3O_4, Si-PVIm-grafted SPION, and Si-Imi were presented in Fig. 3a–c, respectively, which can be used for a quantitative comparison of degradation behavior of different samples. As it was shown in Fig. 3a, pure iron oxide shows no weight loss in the temperature range of TG analysis. On the other hand, degradation is seen in the TGA curves of both Si-Imi and Si-PVIm-grafted SPION. Degradation of Si-Imi over the iron oxide begins at a much lower temperature. This behavior could originate from the fact that iron oxide particles behave as catalysts thus reducing the degradation temperature of Si-Imi. Moreover, temperature range between degradation of Si-Imi is wider than that for the nanocomposite. This result might also be attributed to catalytic effects of nanoparticles for the degradation of Si-Imi. Similar behavior was also observed for degradation of PEG and Carnosine over various nanoparticles (Karaoğlu et al. 2011a, b; Durmus et al. 2011a). Si-PVIm-grafted SPION shows a slight weight loss, while Si-Imi exhibits a considerable thermal stability up to 400 °C. Based on the thermogram, Si-Imi is 25 % of the Si-PVIm-grafted SPION, which means an inorganic content is about 75 %.

TEM analysis

Morphology and particle size of Si-PVIm-grafted SPION were investigated by TEM, and micrographs along with the histogram calculated thereof are given in Fig. 4a, b, respectively. Very small nanoparticles are visible in Fig. 4a. Log-normal fitting of particle size distribution histogram obtained by counting 75 particles from various TEM micrographs (Fig. 4b) yielded an average particle size of 10.0 ± 0.5 nm. Fe_3O_4 particles exhibit near spherical morphology Comparison of crystallite size obtained from X-ray line profile fitting with the particle size observed from TEM suggests that Fe_3O_4-Si-Imi NPs have a mixture of single- and polycrystalline character.

FT-IR analysis

Figure 5a–c shows FT-IR spectra of uncoated magnetite, Si-PVIm, and Si-PVIm-grafted SPION, respectively. The presence of the iron oxide nanoparticles evidenced by the strong absorption bands at around 570–590 cm^{-1} that confirm the metal–oxygen

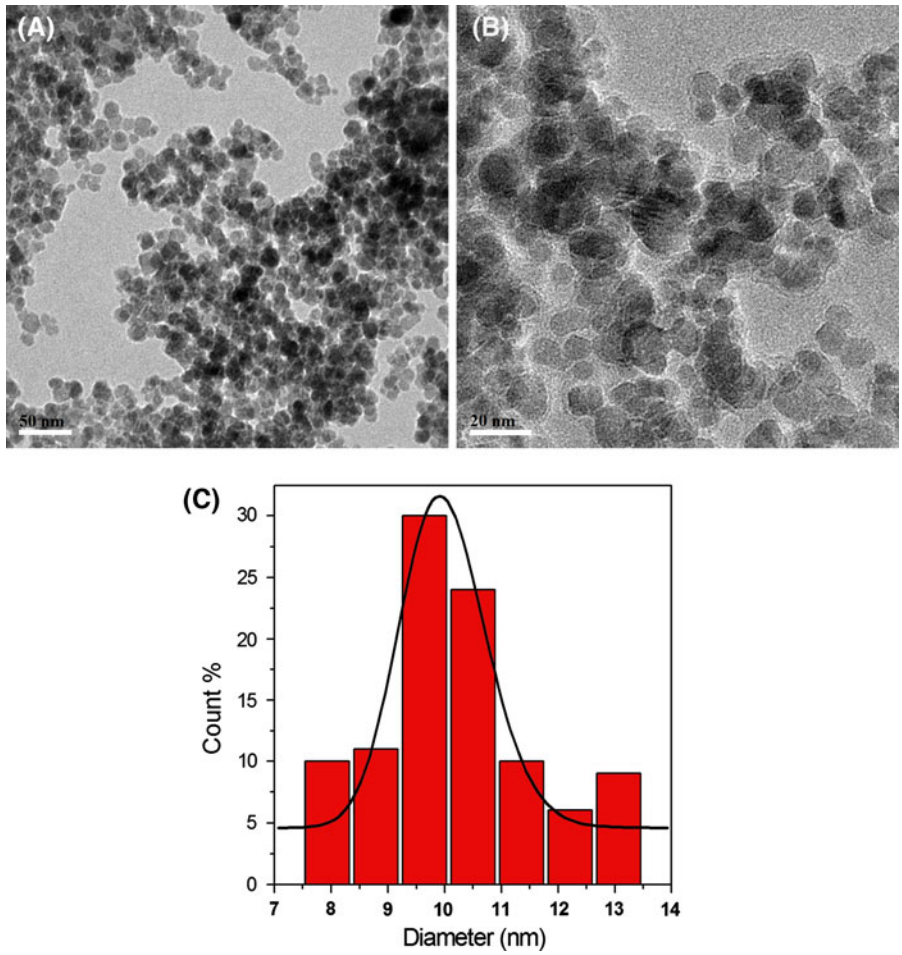

Fig. 4 **a**, **b** TEM micrographs with different magnifications and **c** calculated histogram from several TEM images with log-normal fitting of Si-PVIm-grafted SPION

stretching is present in Fig. 5a, b (Aydin et al. 2012; Karaoğlu et al. 2011c; Ozkaya et al. 2009; Yue et al. 2011; Durmus et al. 2009; Kirwan et al. 2003; Durmus 2009; Bhowmik and Naresh 2010). Figure 5c shows the FT-IR spectra of SPION before and after the immobilization of the Si-PVIm. As shown in this figure, the spectral features of poly(1-vinylimidazole) (Fig. 5a) are observed on Si-PVIm-grafted SPION (Fig. 5c) by the presence of vibration bands at 1496, 1415, and 1225 cm^{-1}, from imidazole cycles, respectively [additionally stretching vibrations of azole C–H (1,100 and 1,080 cm^{-1}) and bending vibrations of heterocycles (917, 827, and 744 cm^{-1})] (Takafuji et al. 2004; Annenkov et al. 2006; Lippert et al. 1985). The presence of peaks around 2,920 and 2,855 cm^{-1} confirmed the presence of C–H group (Kim et al. 2003; Vogt et al. 2010; Unal et al. 2010a; Baykal et al. 2010). The new peak appeared at $\sim$1,000 cm^{-1} after silane modification, which is the characteristic peak for the Si–O bond (Park et al. 2010; Cao et al. 2009; Nguyen et al. 2011). These bands are absent on the spectrum of untreated SPION shown in Fig. 5b.

VSM measurements

Room temperature magnetization curve of Si-PVIm-grafted SPION is shown in Fig. 6. *M–H* hysteresis curve has an immeasurable coercivity and remanence. In addition, magnetization of the samples increases with external magnetic field without reaching to a saturation even at 1.5 T. These are characteristic features of the superparamagnetic nanoparticles. Specific saturation magnetization of the sample is 63 emu/g at 15 kOe. However, this value should be normalized to the weight of the magnetic core which is about 80 % of the total. Then, M_s of the SPION becomes 75.5 emu/g which is still far from the theoretically predicted value

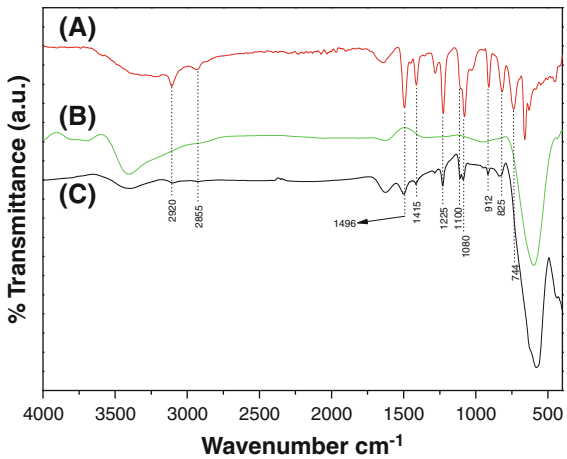

Fig. 5 FT-IR spectra of **a** Si-PVIm, **b** bulk Fe_3O_4 NPs, and **c** Si-PVIm-grafted SPION

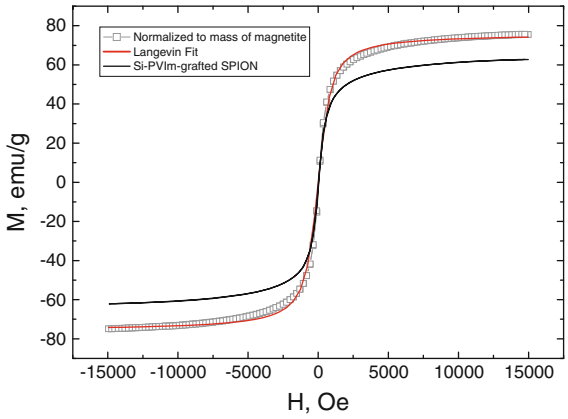

Fig. 6 Room temperature *M–H* hysteresis curve of Si-PVIm-grafted SPION and bulk magnetite which is determined by normalization of the former curve to the mass fraction of the magnetic core. *Solid line* corresponds to a Langevin fit of the measured *M–H* hysteresis curve and is used to determine average particle size

(i.e., 92 emu/g). The possible reason in nanoparticle systems is the difference in spin ordering at the surface of particles over that in the bulk, setting up a magnetic core–shell configuration. Surface effects dominate the properties of the nanoparticles since decreasing the particle size increases the surface to core spin ratio. Surface effects result from the lack of translational symmetry at the boundaries of the particle due to the lower coordination number and existence of broken magnetic exchange bonds which lead to the surface spin disorder and frustration. The magnetization of the Si-PVIm-grafted SPION is further reduced most probably by adsorption of the surfactant molecules to the surface of the magnetite core. This occurs over the oxygen atoms on the surface of SPIONs. Some of the free electrons, i.e., magnetic moments, are used in this process. Hence, reduced M_s can be ascribed to surface spin disorder, canting and adsorption of surfactant molecules to the surface of SPIONs (Kodama et al. 1996a; Batlle and Labarta 2002).

Magnetization of SPIONs can be described by the Langevin function (Eq. 1) which can be used to determine the particle size.

$$M = M_s\left\{\coth\left(\frac{\mu H}{k_B T}\right) - \frac{k_B T}{\mu H}\right\}, \quad (1)$$

where μ denotes the mean magnetic moment of a single particle, H is applied field, and $k_B T$ corresponds to the thermal energy of the particles. The Langevin relation considers each particle as a magnetic monodomain. The relationship, Eq. 2, between the mean magnetic moment of a particle and saturation magnetization of system of particles can be used to calculate average particle size, D.

$$\mu = \frac{M_s \pi \rho D^3}{6}, \quad (2)$$

where ρ is the density of the sample.

Mean magnetic moment, which is used as a fitting parameter, is determined by fitting Eq. 1 to *M–H* hysteresis curve of the composite that is normalized to the bulk mass, as $12{,}602\mu_B$ at 300 K. Then, using this value, mean particle size is found as 8.4 ± 1.0 nm which agrees well with the values calculated from XRD patterns (9 ± 2 nm).

Conductivity measurements

AC conductivity

The alternating current (ac) conductivity of the Si-PVIm-grafted SPION was measured from 20 to 120 °C by means of impedance spectroscopy as a function of frequency and temperature. The frequency-dependent ac conductivity graph of Si-PVIm-grafted SPION is displayed in Fig. 7. Frequency-dependent ac conductivity, $\sigma_{ac}(\omega)$, has been obtained using the following equation:

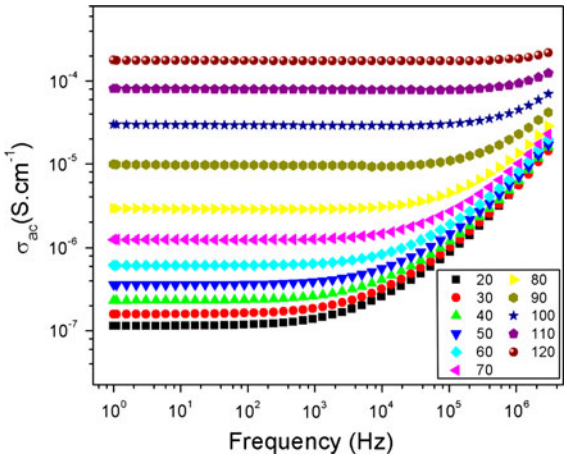

Fig. 7 The variation of ac conductivity of Si-PVIm-grafted SPION as a function of frequency and temperature

$$\sigma'(\omega) = \sigma_{ac}(\omega) = \varepsilon''(\omega)\omega\varepsilon_0 \quad (3)$$

where $\sigma'(\omega)$ is the real part of conductivity, $\omega(=2\pi f)$ is the angular frequency, ε'' is the imaginary part of complex dielectric permittivity (ε^*), and ε_0 (=8.852 × 10 – 14 F cm^{-1}) is the vacuum permittivity.

It is seen from Fig. 7, the curves of ac conductivity versus frequency for various temperatures comprise well-developed conductivity plateau regions particularly at low frequencies at low temperatures, while the conductivity plateau regions broaden toward higher frequencies at higher temperatures. The frequency-dependent ac conductivity curves exhibit a general trend at all temperatures in the log–log plot. Figure 7 shows that ac conductivities increase regularly with temperature and do not show frequency-dependent behavior particularly at lower frequency regime whereas it is strongly temperature dependent. The ac conductivities were measured as 1.2 × 10^{-7} and 1.7 × 10^{-4} S cm^{-1} for 20 and 120 °C at 100 Hz, respectively, while the conductivities were found to be 5.5 × 10^{-6} and 1.97 × 10^{-4} S cm^{-1} at 1 MHz for the same temperatures. It has been shown in previous studies that this phenomenon is a strong indication for ionic conductivity (Baykal et al. 2010; Unal et al. 2010b). The ac conductivity of the nanoparticle increases significantly (more than 10^2 times) with temperature until phase transition temperature of about 65 °C.

This remarkable enhancement in ac conductivity of Si-PVIm-grafted SPION as temperature increases may be described by the increasing mobility of charge carrier sites due to the contribution of the local dynamics and percolation of the nanocomposites.

Initially, Fe_3O_4 nanoparticles surrounded by Si-PVIm can form a random network at low temperatures, and when the temperature is increased gradually, the nanoparticles become more organized and exhibit more capacitive behavior and weak frequency response on hopping conduction which leads to an increase in electrical conductivity. Moreover, Fe_3O_4 nanoparticles may also interact with each other leading a percolated path that electrical current flows through both semiconducting Fe_3O_4 nanoparticles and Si-PVIm with the applied temperature as reported in the literature (Deligöz et al. 2012a; Karaoğlu et al. 2011c; Temizel et al. 2011; Bhattacharyya et al. 2000). This phenomenon can be called as a temperature-assisted formation of the organized X-surrounded magnetite NPs which results in modification of overall conductivities with temperatures. Complete reorganization of the salicylic Si-PVIm-grafted SPION takes place over a temperature of 65 °C. Accordingly, the ac conductivity increases regularly with reciprocal temperature in Arrhenius plot up to 60 °C, and then a transition region takes place at a temperature range of 60–70 °C. It starts to increase again sharply with reciprocal temperature over 70 °C. This is essentially due to the influence of the thermal energy exerted on polymer-like material at about 65 °C. Concerning the frequency dependence of ac conductivity, it is clearly seen that the Si-PVIm-grafted SPION displayed a frequency-dependent conductivity at higher frequencies. The ac conductivity of samples increase linearly with frequency region due to the increases of conductivity of Si-PVIm-grafted SPION at high temperatures particularly over transition temperature of 65 °C and frequency of about 10 kHz, whereas no changes are recorded at low-frequency zone. In other word, the conductivities are comparable at high frequencies particularly at 1 MHz and independent of temperature while it shows a more temperature-dependent behavior at low frequencies. This situation may also be considered as an evidence for ionic conductivity (Unal et al. 2010a). Additionally, the sharply defined power law was proposed to describe the temperature-independent behavior of several low-mobility

polymers and even for crystalline materials, non-crystalline, and liquid semiconductors:

$$\sigma_{ac}(\omega) = A \cdot \omega^{n} \quad (4)$$

where ω is the angular frequency, n is the frequency exponent, and A is a temperature-independent constant (Bouamrane and Almond 2003; Qu et al. 2001). The curves of a low-frequency plateau followed by a power law region at high frequencies can be explained qualitatively with the graphs in Fig. 8, and also the variations of n value with temperature are given in the inset of the figure. Frequency exponent "n" values were calculated from the slopes of log σ_{ac}–log ω graph by fitting the data to Eq. 2, and n values were found to be in the range of 0.06–1.01 for Si-PVIm-grafted SPION. It is clearly seen that frequency exponent n values of nanoparticles significantly decreased with temperature which is in agreement with the previous results reported for amorphous materials (Hallouet et al. 2007; Afandiyeva et al. 2008). The change of n values with temperature is a strong evidence for thermally activated polarization mechanism, as a result the lower n values from the ac measurements can be explained by strong electrode polarization if we suppose that the conduction mechanism is based on ion migration in the applied electric field. Subsequently, it shows us that a kind of temperature-dependent reorganization of Si-PVIm-grafted SPION occurs within the range of phase transition in nanocomposite matrices.

dc conductivity

The variation of direct current (dc) conductivities of Si-PVIm-grafted SPION versus reciprocal temperature is displayed in Fig. 9. The dc conductivities were derived from the well-developed plateau region in graphs of σ_{ac} versus freq. by linear fittings.

As it can be seen from Fig. 9, the dc conductivity curves exhibit significant influence of temperature on conductivity involving a transition region. In general, Si-PVIm-grafted SPION exhibits Arrhenius behavior within the applied temperature range of 20–120 °C providing two different activation energies below and above the transition region. The conductivity isotherm at low and high temperature can be fitted with Arrhenius equation as follows:

$$\log \sigma_{dc} = \log \sigma_0 - E_a/k_B T \quad (5)$$

where σ_{dc} is the dc conductivity, σ_0 is the pre-exponential term, E_a is the activation energy, k_B is the Boltzmann constant (8.617×10^{-5} eV K^{-1}), and T is the temperature in K. The activation energy, E_a, values were calculated from the slope of the curve before (20–65 °C) and after (65–120 °C) transition temperature region, and E_a values were found to be $E_{a1} = 0.152$ and $E_{a2} = 0.517$ eV, respectively. The Si-PVIm-grafted SPION shows better conductivities as compared with similar work though it has higher activation energies (Deligöz et al. 2012). The reason of this relative higher conductivity can be interpreted as

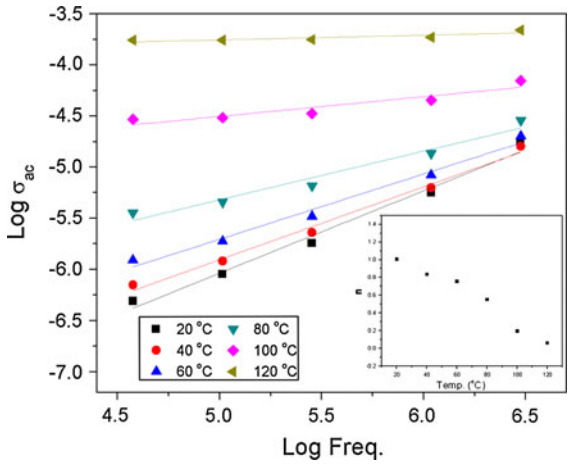

Fig. 8 Plots of log σ_{ac} versus log ω_{max} of Si-PVIm-grafted SPION

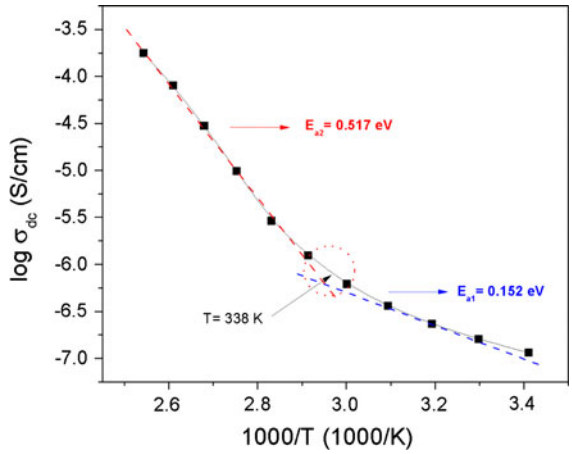

Fig. 9 The variation of dc conductivity and n versus inverse temperature (*inset*) of Si-PVIm-grafted SPION

having lower transition temperature zone; therefore, conductivity increases significantly and exhibits remarkable difference as compared with previous work at same temperature above transition regime.

Permittivity

The frequency and temperature-dependent complex permittivity parameters, real (ε') and imaginary (ε'') parts, of Si-PVIm-grafted SPION in the frequency range $1–3 \times 10^6$ Hz and temperature range 20–120 °C are shown in Figs. 10 and 11, respectively. In general, the real part of permittivity of the nanoparticles exhibits a sharp exponential decay with frequency at low-frequency range at low temperatures, while the decline in real part is relatively slow at higher temperatures and frequencies, and also the actual intensity at this frequency range is quite low. This expected consequence is certainly due to the reorganization of nanocomposite at high-temperature range as a whole and phase transition (65 °C) when passed through the medium temperature range (Durmus et al. 2011a). It shows a slight curvature over transition temperature around 1 kHz. The curves retained their shapes, however, shifted slightly to higher frequencies with temperature. It is a typical behavior for polymers or polymer-like materials that ε' decreases constantly with increasing frequency which has been also observed for Si-PVIm-grafted SPION. The variation of real part of dielectric permittivity at higher frequency regime is quite small which can be described by frequency dependence of the polarization mechanisms. It is known that dielectric constant is correlated to how fast the polarizable units in a polymer orient to keep up with the oscillations of an applied alternating electric field. The orientational polarization decreases with increasing frequency, because the orientation of dipole moments requires a longer time than electronic and ionic polarizations that result in a significant decline in the real part of dielectric permittivity. Additionally, the variation of ε' with frequency indicates the existence of material electrode interface polarization processes taking place at low frequencies (Ukishima et al. 1997).

In general, the real part of dielectric permittivity increases with temperature due to the molecular orientation and arrangement (Yakuphanoglu et al. 2003). As it can be seen from Fig. 10, real part of dielectric permittivity increases with temperature

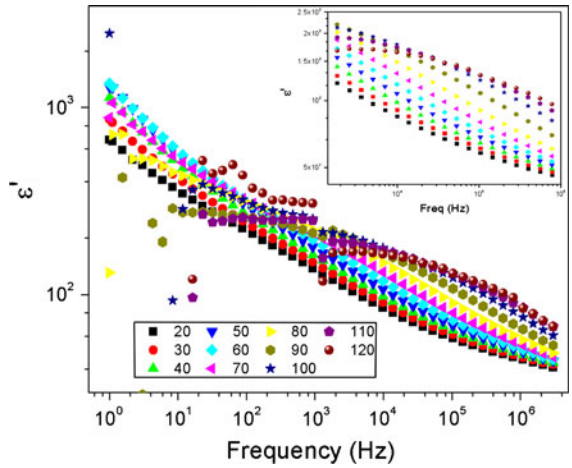

Fig. 10 Real (ε') part of permittivity of Si-PVIm-grafted SPION as a function of frequency at various temperatures

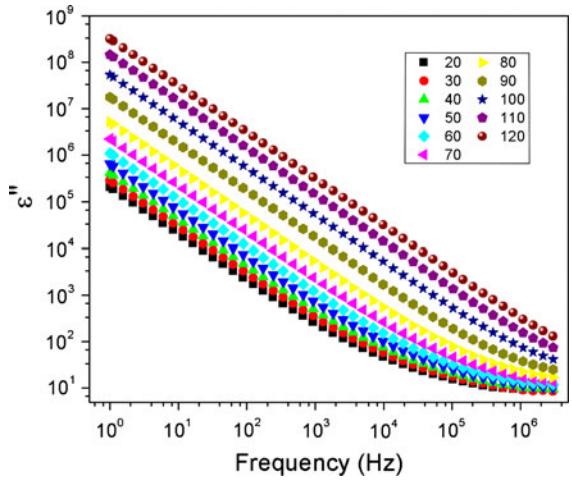

Fig. 11 Imaginary (ε'') part of permittivity of Si-PVIm-grafted SPION as a function of frequency at various temperatures

because of the development of interfaces between Si-PVIm and SPION as reported in the literature. As a result, real part of dielectric permittivity of Si-PVIm-grafted SPION increases markedly until the temperature of about 80 °C, and then increment lessens or ε' slightly declines beyond this temperature particularly at lower frequencies. It is also known that silane bonds are quite flexible which may lead Si-PVIm-grafted SPION to behave as rubber-like as a result nanoparticles may readily interact with each other providing a percolated path that will assist the conduction. Subsequently, the dielectric constant increases usually with temperature as seen in semiconductors. The

thermal energy converts the bound charges to the charge carriers causing an increase in charge carrier concentration which always leads to easy alignment of dipoles in the applied ac electrical field and accordingly increases in dielectric constants. It should be also emphasized that the mobility of the charge carriers enhances by elevating the temperature because of the increase in thermal energy.

The variations of imaginary part of the permittivity, called as dielectric loss (ε"), with frequency are displayed in Fig. 11. It is clearly seen that ε" of Si-PVIm-grafted SPION decreases linearly with frequency and reaches a minimum which becomes more considerable at lower temperatures. It should be noted that Si-PVIm-grafted SPION system comprises a heterogeneous double structure having the highly conducting grains which are separated by moderately poor conducting grain boundaries. The grain boundaries are effective at lower frequencies and the grains at higher frequencies (Batoo et al. 2009). Regarding the polarization mechanism, therefore, more energy is required for the polarization in the grain boundaries at lower frequencies which results in high-energy loss, whereas less energy is required for polarization in the grains and causing small energy loss at high frequencies. Consequently, interface polarization is leading at lower frequencies, while other mechanisms such as electronic and ionic exist at higher frequencies (Deligöz et al. 2012; Iqbal and Ismail 2010; Unal et al. 2011; Tsangaris et al. 1998). The imaginary part of permittivity turns out to be less sensitive to both frequency and temperature, and stays nearly same at high frequency (100 kHz–3 MHz) particularly at lower temperatures as reported earlier (Mürbe et al. 2008).

Electrical modulus

To study the influence of polarization on conductivity of nanoparticles, electrical modulus formalism is a quite versatile method. The real (M') and imaginary (M'') part of the complex dielectric modulus versus frequency are presented in Figs. 12 and 13, respectively.

The real and imaginary components of electrical modulus are calculated using ε' and ε'' data (Batlle and Labarta 2002; Kodama et al. 1996a, b; Durmus et al. 2011b, c):

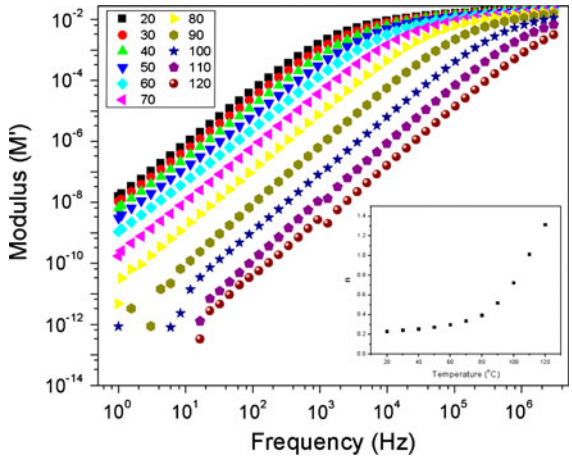

Fig. 12 Real part of modulus (M') of Si-PVIm-grafted SPION as a function of frequency at various temperatures

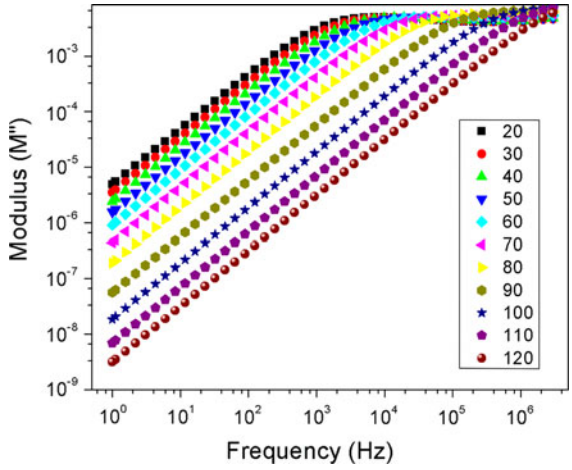

Fig. 13 Imaginary part of modulus (M'') of Si-PVIm-grafted SPION as a function of frequency at various temperatures

$$M^* = \frac{1}{\varepsilon^*} = M' + iM'' \rightarrow M^* = \frac{\varepsilon' + i\varepsilon''}{\varepsilon'^2 + \varepsilon''^2} \quad (6)$$

At low frequency, the variation of dielectric constant with frequency shows the presence of material electrode interface polarization processes. The frequency dependence of ac conductivity follows the universal power law with a small deviation in the low-frequency region according to the equation $M'(T,\omega) = M'_0(T)\omega^n$, where n changes from 0.23 to 1.32 with variation of temperature (Fig. 12, inset). The change of n with temperature is a strong suggestion for polarization effect. The frequency dependency of real part of modulus persist up to 1 kHz for a temperature

of 20 °C, while it shows this dependency up to 1 MHz for 120 °C. If we go to higher frequencies, the change of M' becomes insignificant or remains nearly constant for all temperatures which is consistent with previously reported studies (Deligöz et al. 2012b; Mott and Davis 1979; Coey and Khalafalla 1972).

The imaginary part (M'') is a useful way in order to suppress the effect of electrode polarization at lower frequencies. The imaginary part of electrical modulus increases regularly with temperature particularly at low-temperature regime, and then it shows a maximum which shifts to higher frequencies (from 1 kHz to 1 MHz) at higher temperatures. This non-Debye behavior is a consequence of distributions of relaxation time and because of non-exponential approach of electrical functions. In other words, it may be assigned to the temperature-assisted reorganization effect due to the remarkable structural difference of nanoparticles. The maximum of the peaks indicates the conductivity relaxation times and as a consequence related to the conductivity. It can be concluded from the plot that the polarization effect on this nanoparticle is unavoidable.

Conclusions

In this study, Si-PVIm-grafted SPION with conducting and magnetic characteristics was synthesized by wet chemical processes for the first time. Si-PVIm has been synthesized in a separate process and was then coated/adsorbed on synthesized magnetite nanoparticles.

The ac conductivity shows a temperature-dependent behavior at low frequencies, whereas it has frequency-dependent behavior at high frequencies. The dc conductivity is strongly temperature dependent and shows two different trends before and after transition zone. Activation energies (E_a) of Si-PVIm-grafted Fe_3O_4 are found to be 0.152 and 0.517 eV in these two different zones, respectively. The variation of n values with temperature confirms thermally activated polarization mechanism. Dielectric measurements suggest that conduction mechanism depends both on temperature and on the nature of the reorganization of the nanocomposite. Dielectric constants increased with temperature and decreased with frequency as seen in semiconductors. The real and imaginary part of electrical modulus increases regularly with temperature, exhibiting a maximum which shifts to higher frequencies.

All the properties found in this nanosystem imply a wide variety of biomedical applications as a very promising drug carrier and bioseparator and metal ions separation from waste water.

Acknowledgments This work is supported by Fatih University under BAP Grant No. P50021104-B.

References

Afandiyeva IM, Dökme I, Altındal S, Tataroglu A (2008) Frequency and voltage effects on the dielectric properties and electrical conductivity of Al–TiW–Pd_2Si/n-Si structures. Microelectron Eng 85:247–252

Annenkov VV, Danişovtseva EN, Filina EA, Likhoshway YV (2006) Interaction of silicic acid with poly(1-vinylimidazole). J Polym Sci A 44:820–827

Aydın M, Ünal B, Esat B, Baykal A, Karaoğlu E, Toprak MS, Sözeri H (2012) Synthesis, magnetic and electrical characteristics of poly(2-thiophen-3-yl-malonic acid)/Fe_3O_4 nanocomposite. J Alloys Compd 514:45–53

Bajaj B, Malhotra BD, Choi A (2010) Preparation and characterization of bio-functionalized iron oxide nanoparticles for biomedical application. Thin Solid Films 519:1219–1223

Batlle X, Labarta A (2002) Finite-size effects in fine particles: magnetic and transport properties. J Phys D 35:15–42

Batoo KM, Kumar S, Lee CG, Alimuddin (2009) Study of dielectric and ac impedance properties of Ti doped Mn ferrites. Curr Appl Phys 9:1345–1397

Baykal A, Bıtrak N, Ünal B, Kavas H, Durmus Z, Özden Ş, Toprak MS (2010) Polyol synthesis of (polyvinylpyrrolidone) PVP–Mn_3O_4 nanocomposite. J Alloys Compd 502:199–207

Bhattacharyya S, Saha SK, Chakravorty D (2000) Conductivity relaxation behavior of interpenetrating polymer network composites of polypyrrole and poly(styrene-co-butyl acrylate). J Polym Sci 38:1193–1200

Bhowmik RN, Naresh N (2010) JIT based quality management: concepts and implications in Indian context. Int J Eng Sci Technol 2:40–52

Bouamrane R, Almond P D (2003) The 'emergent scaling' phenomenon and the dielectric properties of random resistor–capacitor networks. J Phys Condens Matter 15:4089

Butterworth MD, Illum L, Davis SS (2001) Preparation of ultrafine silica- and PEG-coated magnetite particles. Colloids Surf A 179:93–100

Cao H, He J, Deng L, Gao X (2009) Fabrication of cyclodextrin-functionalized superparamagnetic Fe_3O_4/amino-silane core–shell nanoparticles via layer-by-layer method. Appl Surf Sci 255:7974–7980

Coey JMD, Khalafalla D (1972) Superparamagnetic γ-Fe_2O_3. Phys Status Solidi A 11:229–241

De M, Chou SS, Joshi HM, Dravid VP (2011) Hybrid magnetic nanostructures (MNS) for magnetic resonance imaging applications. Adv Drug Deliv Rev 63:1282–1299

Deligöz H, Tanrıverdi EE, Durmus Z, Toprak MS (2012a) Synthesis, structural and electrical properties of triethylene glycol (TREG) stabilized $Mn_{0.2}Co_{0.8}Fe_2O_4$ NPs. Mater Res Bull 47:537–543

Deligöz H, Baykal A, Senel M, Sözeri H, Karaoğlu E, Toprak MS (2012b) Synthesis and characterization of poly(1-vinyltriazole)-grafted superparamagnetic iron oxide nanoparticles. Synth Met 162:590–597

Durmus Z (2009) Synthesis and characterization of coated magnetic spinel nanoparticles. Master Thesis, Fatih University of Istanbul, Turkey

Durmus Z, Kavas H, Toprak MS, Baykal A, Altıncekic TG, Aslan A, Bozkurt A, Cosgun S (2009) L-lysine coated iron oxide nanoparticles: synthesis, structural and conductivity characterization. J Alloys Compd 484:371

Durmus Z, Sözeri H, Unal B, Baykal A, Topkaya R, Kazan S, Toprak MS (2011a) Magnetic and dielectric characterization of alginic acid–Fe_3O_4 nanocomposite. Polyhedron 30:322–328

Durmus Z, Erdemi H, Aslan A, Toprak MS, Sozeri H, Baykal A (2011b) Synthesis and characterization of poly(vinyl phosphonic acid) (PVPA)–Fe3O4 nanocomposite. Polyhedron 30:419–426

Durmus Z, Kavas H, Baykal A, Sozeri H, Alpsoy L, Çelik SÜ, Toprak MS (2011c) Synthesis and characterization of L-carnosine coated iron oxide nanoparticles. J Alloys Compd 509:2555–2561

Hallouet B, Wetzel B, Pelster R (2007) On the dielectric and magnetic properties of nanocomposites. J Nanomater 11:1–11

Iqbal MJ, Ismail B (2010) Correlation between structural and electrical properties of $Mg_{1-2x}Zn_xNi_xAl_2O_4$ ceramic nanomaterials synthesized by a urea assisted microwave combustion method. J Alloys Compd 504:440–448

Karaoğlu E, Deligöz H, Sözeri H, Baykal A, Toprak MS (2011a) Hydrothermal synthesis and characterization of PEG–Mn_3O_4 nanocomposite. Nano-Micro Lett 3:25–33

Karaoğlu E, Kavas H, Baykal A, Toprak MS, Sözeri H (2011b) Effect of hydrolyzing agents on the properties of poly (ethylene glycol)–Fe_3O_4 nanocomposite. Nano-Micro Lett 3:79–85

Karaoğlu E, Baykal A, Erdemi H, Alpsoy L, Sozeri H (2011c) Synthesis and characterization of DL-thioctic acid (DLTA)–Fe_3O_4 nanocomposite. J Alloys Compd 509:9218–9225

Kavas H, Durmus Z, Baykal A, Aslan A, Bozkurt A, Toprak MS (2010) Synthesis and conductivity evaluation of PVTri–Fe_3O_4 nanocomposites. J Non-Cryst Solids 356:484–489

Kim DK, Mikhaylova M, Zhang Y, Muhammed M (2003) Protective coating of superparamagnetic iron oxide nanoparticles. Chem Mater 15:1617–1627

Kirwan LJ, Fawell PD, Bronswijk WV (2003) In situ FTIR-ATR examination of poly(acrylic acid)adsorbed onto hematite at low pH. Langmuir 19:5802

Kodama RH, Berkowitz AE, McNiff EJ, Foner S (1996a) Surface spin disorder in $NiFe_2O_4$ nanoparticles. Phys Rev Lett 77:394

Kodama RH, Berkowitz AE, McNiff EJ Jr, Foner S (1996b) Surface spin disorder in $NiFe_2O_4$ nanoparticles. Phys Rev Lett 77:394–397

Lippert JL, Robertson JA, Havens JR, Tan JS (1985) Structural studies of poly(*N*-vinylimidazole) complexes by Infrared and Raman Spectroscopy. Macromolecules 18:63–67

Mott NF, Davis EA (1979) Electronic processes in non-crystalline. Clarendon Press, Oxford

Mürbe J, Rechtenbach A, Töpfer T (2008) Synthesis and physical characterization of magnetite nanoparticles for biomedical applications. Mater Chem Phys 110:426–433

Nguyen VH, Haldorai Y, Pham QL, Shim JJ (2011) Supercritical fluid mediated synthesis of poly(2-hydroxyethyl methacrylate)/Fe_3O_4 hybrid nanocomposite. Mater Sci Eng B 176:773–778

Nishio K, Ikeda M, Gokon N, Tsubouchi S, Narimatsu H, Mochizuki Y, Sakamoto S, Sandhu A, Abe M, Handa H (2007) Preparation of size-controlled (30–100 nm) magnetite nanoparticles for biomedical applications. J Magn Magn Mater 310:2408–2410

Ozkaya T, Toprak MS, Baykal A, Kavas H, Köseoglu Y, Aktas B (2009) Synthesis of Fe_3O_4 nanoparticles at 100 °C and its magnetic characterization. J Alloys Compd 472:18–23

Park JO, Rhee KY, Park SJ (2010) Silane treatment of Fe_3O_4 and its effect on the magnetic and wear properties of Fe_3O_4/epoxy nanocomposites. Appl Surf Sci 256:6945–6950

Paulsen JA, Ring AP, Lo CCH, Synder JE, Jiles DC (2004) Presentation W27-5. In: American Physical Society March Meeting, Montreal

Pielaszek R (2003) Applied crystallography. In: Proceedings of the XIX conference, Krakow, Poland

Qu W, Ko TM, Vora RH, Chung TS (2001) Effect of polyimides with different ratios of para- to meta- analogous fluorinated diamines on relaxation process. Polymer 42:6393–6401

Setyawan H, Fajaroh F, Widiyastuti W, Winardi S, Lenggoro IW, Mufti N (2012) One-step synthesis of silica-coated magnetite nanoparticles by electrooxidation of iron in sodium silicate solution. J Nanopart Res 14: 807–815

Takafuji M, Ide S, Ihara H, Xu Z (2004) Preparation of poly(1-vinylimidazole)-grafted magnetic nanoparticles and their application for removal of metal ions. Chem Mater 16:1977–1983

Temizel E, Ayan E, Şenel M, Erdemi H, Yavuz MS, Kavas H, Baykal A, Öztürk R (2011) Synthesis, conductivity and magnetic properties of poly(*N*-pyrrole phosphonic acid)–Fe_3O_4 nanocomposite. Mater Chem Phys 131:284–291

Tsangaris GM, Psarras OC, Kouloumbi N (1998) Electric modulus and interfacial polarization in composite polymeric systems. J Mater Sci 33:2027–2034

Ukishima S, Iijima M, Sato M, Takahashi Y, Fukada E (1997) Heat resistant polyimide films with low dielectric constant by vapor deposition polymerization. Thin Solid Films 475:308–309

Unal B, Durmus Z, Baykal A, Sözeri H, Toprak MS, Alpsoy L (2010a) L-histidine coated iron oxide nanoparticles: synthesis, structural and conductivity characterization. J Alloys Compd 505:172–178

Unal B, Durmus Z, Kavas H, Baykal A, Toprak MS (2010b) Synthesis, conductivity and dielectric characterization of salicylic acid–Fe_3O_4 nanocomposite. Mater Chem Phys 123:184

Unal B, Durmus Z, Baykal A, Toprak MS, Sozeri H, Bozkurt A (2011) Synthesis, dielectric and magnetic characteristics of

poly(1-vinyl-1,2,4-triazole) (PVTri)–barium hexaferrite. J Alloys Compd 509:8199–8206

Uzun K, Cevik E, Şenel M, Sözeri H, Baykal A, Abasıyanık MF, Toprak MS (2010) Covalent immobilization of invertase on PAMAM dendrimer modified superparamagnetic iron oxide nanoparticles. J Nanopart Res 12:3057–3067

Vogt C, Toprak MS, Muhammed M, Laurent S, Bridot JL, Müller RN (2010) High quality and tunable silica shell–magnetic core nanoparticles. J Nanopart Res 12: 1137–1147

Wejrzanowski T, Pielaszek R, Opalińska A, Matysiak H, Lojkowski W, Kurzydlowski KJ (2006) Quantitative methods for nanopowders characterization. Appl Surf Sci 253: 204–208

Yakuphanoglu F, Aydogdu Y, Schatzschneider U, Rentschler E (2003) Electrical conductivity, dielectric permittivity and thermal properties of the compound aqua[bis(2-dimethylaminomethyl-4-NIT-phenolato)] copper(II) including NaCl impurity. Physica B 334:443–450

Yang H, Zhuang Y, Hu H, Du X, Zhang C, Shi X, Wu H, Yang S (2010) Silica-coated manganese oxide nanoparticles as a platform for targeted magnetic resonance and fluorescence imaging of cancer cells. Adv Funct Mater 20:1733–1741

Yuan S, Pehkonen SO, Liang B, Ting YP, Neoh KG, Kang ET (2010) Poly(1-vinylimidazole) formation on copper surfaces via surface-initiated graft polymerization for corrosion protection. Corros Sci 52:1958–1968

Yue FJ, Wang S, Lin L, Zhang FM, Li CH, Zuo JL, Du YW, Wu D (2011) Large low-field magnetoresistance in Fe_3O_4/molecule nanoparticles at room temperature. J Phys D 44:25001–25006